Desalination and Water Treatment
www.deswater.com
doi: 10.1080/19443994.2015.1088808

57 (2016) 16495–16506
July

Taylor & Francis
Taylor & Francis Group

$MnFe_2O_4$ nano spinels as potential sorbent for adsorption of chromium from industrial wastewater

Naim Sezgin[a], Arzu Yalçın[a,*], Yüksel Köseoğlu[b]

[a]*Faculty of Engineering, Department of Environmental Engineering, Istanbul University, Istanbul, Avcilar 34320, Turkey, Tel. +90 212 473 70 70, ext. 17721; email: nsezgin@istanbul.edu.tr (N. Sezgin), Tel. +90 212 473 70 70, ext. 17731; Fax: +90 212 473 71 80; email: temizsoy@istanbul.edu.tr (A. Yalçın)*
[b]*Faculty of Education, Department of Primary Education, Suleyman Demirel University, Isparta, Cunur 32260, Turkey, Tel. +90 246 211 1000, ext. 3886; email: yukselkoseoglu@sdu.edu.tr*

Received 28 March 2015; Accepted 2 August 2015

ABSTRACT

In this study, nanospinels of $MnFe_2O_4$ were synthesized by a rapid method of microwave-assisted combustion technique for the removal of total chromium from real industrial wastewater. Nanoparticles of $MnFe_2O_4$ were characterized by X-ray diffraction and scanning electron microscopy. The removal of total chromium from real industrial wastewater, which was taken from galvanotechnic industry, using of nanospinel $MnFe_2O_4$ was investigated. The effects of adsorbent dosage, contact time, and initial concentrations on total chromium removal from wastewater were studied using the real wastewater. Optimal conditions were found for total chromium removal. Chromium removal and adsorption capacity of $MnFe_2O_4$ nanoparticles (NPs) were achieved as 59.35% and 89.18 mg/g, respectively. In addition, other optimum conditions of adsorbent dosage and contact time were found as 1.5 g/L and 120 min in this study, respectively. The removal of total chromium using $MnFe_2O_4$ NPs was fitted with Freundlich isotherm and pseudo-second-order kinetic models. The results indicated that $MnFe_2O_4$ nanospinels are suitable adsorbents for the removal of total chromium from industrial wastewater.

Keywords: Adsorption; Total chromium; Manganese ferrite; Nanoparticle; Real wastewater treatment

1. Introduction

The pollution of water with toxic heavy metals is considered dangerous due to their great toxicity and nonbiodegradability. These heavy metal ions can be accumulated through the food chain even at low concentrations which leads to serious problems for aquatic life as well as for human health, plant life, and animals [1–3]. Heavy metals are discharged to receiving environments from various industrial production processes such as electric plating, mining, refining, printing, and dyeing [4,5].

One of the important metal pollutants is chromium, due to its widespread use in industrial processes and exceedingly toxic nature [6]. Chromium has long been used in electroplating, leather tanning, metal finishing, nuclear power plants, and textile industries [7]. Among its several oxidation states,

*Corresponding author.

trivalent (Cr^{3+} and $CrOH^{2+}$) and hexavalent ($HCrO_4^-$ and $Cr_2O_7^{2-}$) species of chromium are mainly found in these industrial effluents [8,9]. Chromium leads to serious health problems to human beings such as headache, nausea, diarrhea, carcinogen, and lung tumors [10,11]. Therefore, the removal of chromium from wastewater is nowadays recognized as a key process for the protection of aquatic and terrestrial environments, public health, and well-being [12].

There are various techniques to remove chromium from aqueous solutions such as chemical precipitation, reverse osmosis, adsorption, membrane separation, electrochemical methods, and ion exchange in order to diminish the pollution impact of these metals [13–15]. Of these strategies, adsorption is one of the most recommended physicochemical treatment processes due to some of its characteristics like simple operation, high efficiency, fast response, and low price [16,17]. There are ongoing researches on the use of adsorbents and adsorption methods for heavy metal removal from industrial wastewater, with the aim of finding affordable, efficient, and widely applicable method that generates low amounts of sludge [18,19]. Table 1 shows the main advantages and disadvantages of various physicochemical processes used for the removal of heavy metals from wastewater [20].

The adsorbents to be used in adsorption methods may include synthetic or natural zeolites, biosorbents, clay minerals, activated carbon, fly ash, hydrogels, and nanoparticles [2,20–24]. Nanomaterials such as nanometal oxides [25–29], carbon nanotubes [30], and magnetic nanoparticles [3,27,31,32] have been investigated as available materials to be used for the adsorption of heavy metals due to their special properties, such as easy operation and easy production, high adsorption capacity and unsaturated surfaces [25,33]. Recently, nanostructured materials have been suggested as efficient, easy production and low-cost, easy separation and environmentally friendly alternative adsorbents to existing treatment materials [34–38].

In this study, the removal of total chromium from industrial real (competitive) wastewater was studied using manganese ferrite ($MnFe_2O_4$) nanoparticles (NPs). Manganese ferrite nanoparticles were synthesized by a simple microwave-induced combustion method and being used as adsorbent for total chromium removal. This technique was chosen because it is easy, simple, and cheap to produce large amount of nanoparticles [39,40]. Wastewater samples were used to investigate the effect of adsorbent dosage and contact time on total chromium removal under batch conditions. Langmuir, Freundlich, Dubinin–Radushkevich, and Temkin isotherms were used to analyze the experimental data. The adsorption kinetics was tested for the pseudo-first-order and pseudo-second-order kinetic models.

2. Materials and methods

2.1. Wastewater samples and synthesis of manganese ferrite ($MnFe_2O_4$) NPs

$MnFe_2O_4$ NPs were synthesized through a microwave-induced combustion synthesis route as previously described in the literature [39–42]. All the reagents used in the experiments were analytically pure and were purchased from Merck Chemicals Company, and they were used as received without further purification. Stoichiometric amounts of manganese nitrate [$Mn(NO_3)_2{\cdot}6H_2O$], ferric nitrate [$Fe(NO_3)_3{\cdot}9H_2O$], and urea were each dissolved in 10 mL of deionized water to form a clear solution and mixed altogether. The mixture was stirred with a magnetic stirrer until the reactants were dissolved completely and poured into a crucible, which was then placed in a domestic microwave oven (operating at 2.45 GHz,

Table 1
Comparisons of various physicochemical processes used for the removal of heavy metals from wastewater [20]

Physical and/or chemical methods	Advantages	Disadvantages
Chemical precipitation	Low capital cost, simple operation	Sludge generation, extra operational cost for sludge disposal
Membrane filtration	Small space requirement, low pressure, high separation selectivity	High operational cost due to membrane fouling
Adsorption	Low-cost, easy operating conditions, having wide pH range, high metal binding capacities	Low selectivity, production of waste products
Electrodialysis	High separation selectivity	High operational cost due to membrane fouling and energy consumption
Photocatalysis	Removal of metals and organic pollutant simultaneously, less harmful by-products	Long duration time, limited applications

800 W). Initially, the solution boils and undergoes dehydration followed by decomposition with the evolution of large amount of gases. After the solution reaches the point of spontaneous combustion, it begins burning and releases lots of heat, vaporizes all the solution instantly, and becomes a solid. Here, urea serves as fuel for the combustion reaction, being oxidized by nitrate.

The wastewater samples, which were real and competitive industrial wastewater, were collected from the inflow of a treatment plant of galvanotechnic industrial site in Istanbul for this study. The heavy metal concentrations included by the wastewater samples are given in Table 2. In addition, the original pH value of used wastewater was 2.

For the structural characterization and phase identification of the product, X-ray powder diffraction (XRD) analysis was conducted on a Rigaku Smart Lab diffractometer operated at 40 kV and 35 mA using Cu Kα radiation. Field emission scanning electron microscopy (FE-SEM, JEOL 7001 FE) was used in order to investigate the nanostructure and morphology of the as-synthesized sample. The sample was coated with carbon prior to scanning electron microscopy (SEM) analysis.

In addition, specific surface area of $MnFe_2O_4$ NPs was measured using a NOVA3200 E analytical system made by Quantachrome Instruments (USA). The specific surface area was calculated by Burnauer–Emmett–Teller (BET) N_2 method.

2.2. Experimental procedures

The wastewater was filtered with a mesh size of 0.45 μm prior to experiments. In batch tests, 20 mL synthetic and industrial wastewater samples were placed in 100-mL Erlenmeyer flasks; adsorbent was added and the flasks were shaken at 150 rpm in a shaker (Gallenkamp orbital incubator). The samples were filtered with a mesh size of 0.22 μm and then transferred to glass tubes for analysis. The total chromium concentrations in solutions before and after adsorption were measured using atomic absorption spectroscopy (AAS, Perkin–Elmer Analyst 400). All the adsorption experiments were conducted at room temperature.

Table 2
Heavy metal concentrations in the sample wastewater

Cations	Concentration (mg/L)
Cu^{2+}	86.12
Ni^{2+}	83.99
Zn^{2+}	178.30
Total Cr	302.80
Total Fe	77.74
Na^{+}	822.88
NH_4^{+}	181.23
K^{+}	146.81
Mg^{2+}	59.01
Ca^{2+}	212.22

The total chromium removal and adsorption capacities of manganese ferrite ($MnFe_2O_4$) NPs were calculated by means of Eqs. (1) and (2), respectively.

$$\text{Removal efficiency} = \frac{(C_0 - C_e)}{C_0} \times 100 \quad (1)$$

$$q = \frac{(C_0 - C_e)}{m} \times V \quad (2)$$

where C_0 represents the initial concentration of metal in the wastewater (mg/L); C_e is metal concentrations in the solution after the experiment (mg/L); q is the equilibrium adsorption capacity (mg/g); V is the sample volume (L) and m is the amount of $MnFe_2O_4$ NPs used (g).

The effects of adsorbent dosages, contact times, and initial total chromium concentrations on chromium adsorption were evaluated. For this purpose, experiments were carried out at adsorbent dosages of 0.5, 1.0, 1.5, 2.0, 3.0, and 6.0 g/L, contact times 10–1,440 min, and initial total chromium concentrations varying from 50 mg/L to 250 mg/L in the wastewater samples.

2.3. Adsorption isotherm

Adsorption isotherm is useful to describe how solutes interact with adsorbents and very important to evaluate the feasibility of the adsorbate–adsorbent system. The isotherm data explained by theoretical or empirical equations provide preliminary prediction in modeling steps which is desired to practical operation [43].

In order to determine the adsorption isotherm model Langmuir, Freundlich, Dubinin–Radushkevich, and Temkin equations were used. These models are widely used in adsorption modeling processes. The linear form of the Langmuir isotherm is as follows [44] (Eq. (3)):

$$\frac{C_e}{q_e} = \frac{1}{K_L q_m} + \frac{C_e}{q_m} \quad (3)$$

where C_e is the equilibrium concentration of the adsorbate (mg/L); q_e is the amount of adsorbate

adsorbed per unit mass of adsorbent at equilibrium (mg/g); q_m is the theoretical maximum monolayer adsorption capacity of the adsorbent (mg/g); K_L is the Langmuir isotherm constant related to the adsorption energy (L/mg), the relationship between the adsorbent and the adsorbate. The values of q_m and K_L can be determined from the slope and intercept of the linear plot of C_e/q_e vs. C_e.

The Freundlich isotherm is expressed in linear form as follows [45] (Eq. (4)):

$$\log q_e = \log K_F + \left(\frac{1}{n}\right) \log C_e \tag{4}$$

where K_F is the Freundlich isotherm constant related to the adsorption capacity of the adsorbent (mg/g), and $1/n$ is the adsorption intensity that ranges between 0 and 1, where zero represents maximum heterogeneity of adsorbent surface. $1/n$ gives an indication of the favorability of adsorption. The values of K_F and $1/n$ were calculated from the intercept and slope of the plot of $\ln q_e$ vs. $\ln C_e$.

In order to express the adsorption mechanism generally, Dubinin–Radushkevich isotherm is applied with a Gaussian energy distribution onto a heterogeneous surface [46,47]. The model has often successfully fitted high solute activities and the intermediate range of concentrations data well. A linear form of the Dubinin–Radushkevich isotherm is as follows (Eq. (5)):

$$\ln q_e = \ln q_d - \beta\varepsilon^2 \tag{5}$$

where q_e is the amount of adsorbate in the adsorbent at equilibrium (mg/g); q_d is the theoretical isotherm saturation capacity (mg/g); β is the Dubinin–Radushkevich isotherm constant related to sorption the mean free energy (mol^2/kJ^2); ε is the Polanyi potential, which is related to equilibrium concentration as follows (Eq. (6)):

$$\varepsilon = RT \ln\left(1 + \frac{1}{C_e}\right) \tag{6}$$

where R is the gas constant (8,314 J/mol K) and T is the absolute temperature. The approach was usually applied to distinguish the physical and chemical adsorption of metal ions with its mean free energy, E per molecule of adsorbate (for removing a molecule from its location in the sorption space to the infinity) can be computed by the relationship [48] (Eq. (7)):

$$E = \frac{1}{\sqrt{2\beta}} \tag{7}$$

The value of q_d and β was calculated from the intercept and slope of the plot of $\ln q_e$ vs. ε^2.

In addition, the Temkin isotherm contains a factor that explicitly takes into account the adsorbing species–adsorbate interactions; the isotherm is given by a linearized expression as [49] (Eq. (8)):

$$q_e = B_T \ln K_T + B_T \ln C_e \tag{8}$$

where $B_T = RT/b$ (R is the universal gas constant (8.314 J/mol K), T is temperature (K), B_T is the Temkin constant related to adsorption energy (kJ/mol), and K_T is the binding constant at equilibrium corresponding to the maximum binding energy (L/mg). The values of K_T and B_T were calculated from the intercept and slope of the plot of q_e vs. $\ln C_e$.

2.4. Adsorption kinetics

In order to determine the kinetic model of adsorption systems, pseudo-first-order and pseudo-second-order kinetic model equations developed by Lagergren are used (1898) [50]. The linear form of pseudo-first-order kinetic model equation can be expressed as follows [50,51] (Eq. (9)):

$$\ln(q_e - q_t) = \ln q_e - k_1 t \tag{9}$$

where q_t and q_e are the adsorption amounts of heavy metal ions per gram of adsorbent at time t (min) and at equilibrium (mg/g), respectively; k_1 is the rate constant of pseudo-first-order adsorption (min^{-1}); t is the time (min). The equilibrium adsorption capacity q_e and the adsorption rate constant k_1, calculated from the slopes and intercepts of plots of $\log(q_e - q_t)$ vs. t.

The linear form of the pseudo-second-order kinetic model equation is expressed as follows [50,51] (Eq. (10)):

$$\frac{t}{q_t} = \frac{1}{q_e} t + \frac{1}{k_2 q_e^2} \tag{10}$$

where k_2 is the equilibrium rate constant of pseudo-second-order adsorption (g/mg min). The adsorption

rate constant k_2 and equilibrium adsorption capacity q_e, calculated from the slopes and intercepts of plots of t/q_t vs. t.

When q_e values are calculated using experimental data correlate with theoretical values and according to correlation coefficient (R^2) values, adsorption rate is deemed to fit the pseudo-first or second-order kinetic models.

Also, the adsorption data were subject to piecewise linear regression analysis to understand the mechanism of adsorption. The information related to adsorption mechanism can be used to optimize the design of adsorption conditions and adsorbents [52]. The following three steps can be used to describe the overall rate of adsorption [53]: (1) surface or film diffusion where the sorbate is transported from the bulk solution to the external surface of sorbent, (2) pore or intra-particle diffusion, where sorbate molecules move into the interior of sorbent particles, and (3) adsorption on the interior sites of the sorbent. It is assumed that the adsorption step does not influence the overall kinetics because it is very rapid. Therefore, the overall rate of adsorption process can be controlled by either surface diffusion or intra-particle diffusion. If the intra-particle diffusion is the rate-limiting step, the Weber–Morris intra-particle diffusion model has often been used to determine it as the following equation [54,55] (Eq. (11)):

$$q_t = k_i t^{0.5} + C \tag{11}$$

where k_i is the intra-particle diffusion rate constant ((mg/g) $\text{min}^{0.5}$) and C is the intercept. According to this model, if intra-particle diffusion is involved in the adsorption process, the plot of q_t vs. $t^{0.5}$ should be linear, and if the plot passes through the origin, then intra-particle diffusion is the sole rate-limiting step [56]. It has also been suggested that in instances when q_t vs. $t^{0.5}$ is multi linear, two or more steps govern the adsorption process [57,58].

3. Result and discussion

3.1. Structural characterization of manganese ferrite NPs

The crystal structure and phase purity of the as-prepared sample of $MnFe_2O_4$ nanospinel was evaluated by powder X-ray diffraction (XRD). Fig. 1 represents the XRD pattern of the as-prepared sample of $MnFe_2O_4$ nanocrystallites. The diffraction peaks confirm the formation of single-phase cubic spinel Mn-ferrite crystal structure without any impurity or secondary phases. The $MnFe_2O_4$ ferrite phase was

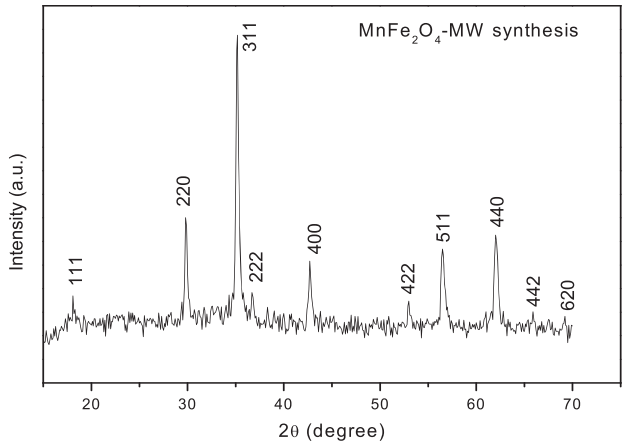

Fig. 1. XRD pattern of as-synthesized $MnFe_2O_4$ nano spinels.

characterized by the main diffraction peaks with the *hkl* values of (1 1 1), (2 2 0), (3 1 1), (2 2 2), (4 0 0), (4 2 2), (5 1 1), (4 4 0) in XRD powder pattern indicated that the XRD pattern of as synthesized sample is identical to pure $MnFe_2O_4$ spinel structure of the standard data (JCPDS file no: 74-2403 for $MnFe_2O_4$) [59,60].

To study the morphology, size and distribution of as-synthesized $MnFe_2O_4$ nanoparticles SEM was used. Field emission scanning electron microscopy (FE-SEM) micrograph of the powder sample is shown in Fig. 2.

From SEM image it is revealed that the sample consists of regular shaped spherical nanoparticles without any signature of phase segregation and agglomeration. A close view of particles also reveals

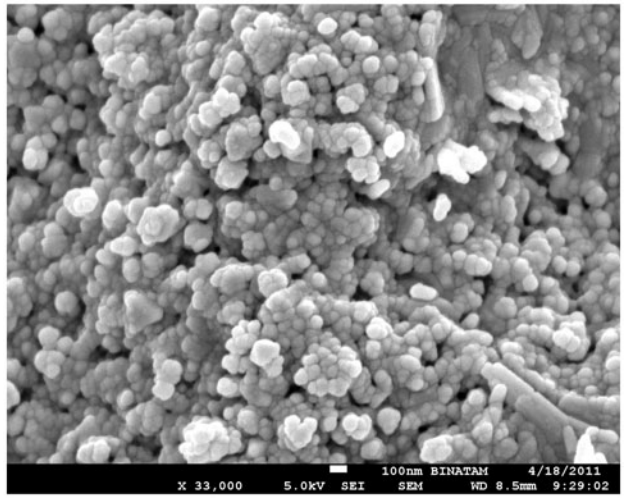

Fig. 2. SEM picture of as-synthesized $MnFe_2O_4$ nano spinels.

that smaller crystallites have sizes less than 100 nm. Nanoparticles were dense and distributed evenly on the whole mass. In addition to this, though these smaller crystallites are so closely arranged together, a clear boundary between neighboring crystallites can still be observed.

Lastly, the specific surface area of the product is found to be 28.95 m^2/g, by using BET.

3.2. Effect of $MnFe_2O_4$ NPs dosage

Fig. 3 shows the effect of $MnFe_2O_4$ dosage on the adsorption of total chromium. As can be seen from the figure, the removal of total chromium was increased with the increase in $MnFe_2O_4$ dosage.

The surface area of the adsorbent increases as the adsorbent dosage increase, as well, more adsorption sites are available to remove chromium from aqueous solution. Therefore, the equilibrium time will be shorter at higher adsorbent dosage as expected [61]. However, adsorption capacities decreased from 334.80 to 34.68 mg/g while adsorbent dosage increased from 0.5 to 6.0 g/L. This behavior is attributed to overlapping or aggregation of adsorbent surface area available to total chromium and an increase in diffusion path length by Garg et al. [61]. The percentage removal of total chromium reached almost a constant value beyond the certain amount of adsorbent (1.5 g). The adsorption capacity and total chromium removal in the presence of 1.5 g/L of $MnFe_2O_4$ NPs were found as 142.90 mg/g and 71.37%, respectively.

3.3. Effect of contact time

The contact time determination is an important parameter for the adsorption kinetics [62,63]. Fig. 4(a) and (b) shows the effect of contact time on total chromium removal.

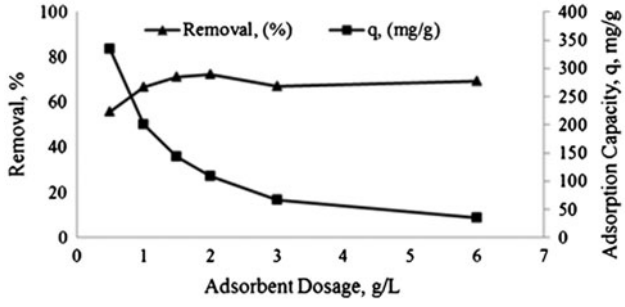

Fig. 3. Effect of adsorbent dosage on total Cr adsorption (conditions: pH 2, contact time = 1,440 min, shaking speed = 150 rpm).

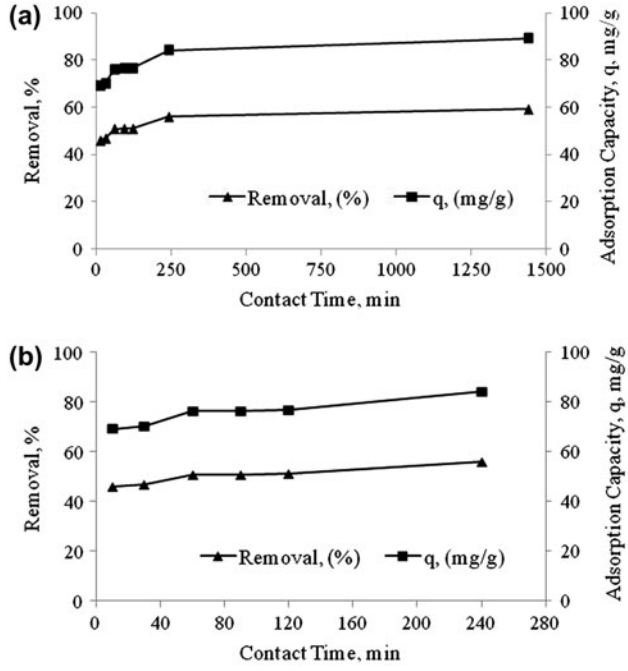

Fig. 4. (a) Effect of contact time on total Cr adsorption, (b) detail figure for 10 and 240 min (conditions: $MnFe_2O_4$ dosage = 1.5 g/L, pH 2, shaking speed = 150 rpm).

As seen in Fig. 4, no significant increase or decrease was found in total chromium removal, and adsorption capacities were found between 10 and 120 min, thereafter these capacities increased slowly (Fig. 4(b), detailed figure for 10 and 240 min). Hence, the equilibrium condition is reached at 120 min and it is chosen as optimal contact time for the subsequent experiments.

3.4. Effect of initial total chromium concentrations

The results of removal of total chromium for different initial concentrations from 50 to 250 mg/L, which were prepared from synthetic solutions, are presented in Fig. 5.

No significant changes occurred for percentage removal of total chromium but the amount of total chromium adsorbed per unit mass of adsorbent increased with increasing initial chromium concentrations as seen from Fig. 5. To overcome all mass transfer resistance of chromium ions between the aqueous and solid phases, the initial chromium concentration is an important driving force; hence, the adsorption capacity can be increased by higher initial concentration of chromium ions. Ozer et al. [64] reported that all available metal ions in the solution could interact with the binding sites at lower concentrations and

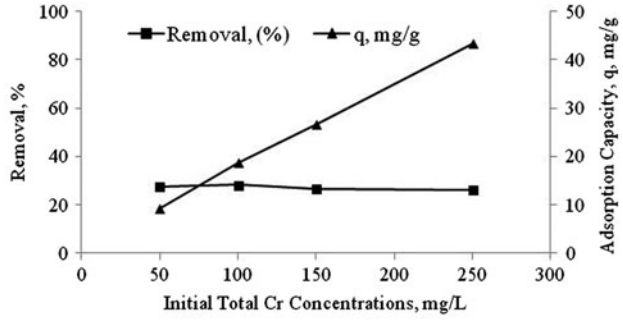

Fig. 5. Effect of initial concentrations varying from 50 to 250 mg/L on total Cr adsorption (conditions: $MnFe_2O_4$ dosage = 1.5 g/L, contact time = 1,440 min, shaking speed = 150 rpm).

thus the percentage adsorption was higher than those at higher initial metal ion concentrations. At higher concentrations, lower adsorption yield can be found from the saturation of adsorption sites.

3.5. Adsorption isotherms

The adsorption isotherm models such as Langmuir, Freundlich, Dubinin–Radushkevich, and Temkin were applied to data of total chromium adsorption. The correlation coefficients of the Langmuir, Freundlich, Temkin, and Dubinin–Radushkevich isotherms were found as 0.756, 0.997, 0.955, and 0.876, respectively. The adsorption isotherms constant and correlation coefficients for different isotherm model are given in Table 3.

According to the linear coefficients of determination (R^2) given in Table 3, the total chromium adsorption is better fitted to Freundlich and Temkin isotherms model. In order to determine the most appropriate isotherm model, chi-square (χ^2) test was performed to isotherm models using the mathematical expression as follows [65] (Eq. (12)).

$$\chi^2 = \sum \frac{(q_{e,cal} - q_e)^2}{q_{e,cal}} \quad (12)$$

where $q_{e,cal}$ is the equilibrium capacity (mg/g) calculated from model and q_e is the equilibrium capacity (mg/g) obtained from the experimental data. The value of $q_{e,cal}$ and chi-square (χ^2) as calculated from four isotherms are depicted in Table 4.

It can be seen from Table 3 that the linear form of Freundlich and Temkin adsorption isotherm models regression coefficient (R^2) values are more than 0.95. On the other hand, as seen in Table 4 that $q_{e,cal}$ values of Freundlich isotherm model have closer q_e than the Temkin isotherm $q_{e,cal}$ values. In addition, the total value of (χ^2) Freundlich isotherm is smaller than the Temkin isotherm. Thus, in both, linear and nonlinear form, Freundlich adsorption isotherm model found to be more accurate model. Thus, total chromium adsorption is better fitted to the Freundlich model. Accordingly, it is assumed that adsorption sites on the adsorbent surface are heterogeneous and there was no interaction between the molecules adsorbed onto the surface [66]. Furthermore, K_F and n values in the Freundlich isotherm, parameters, and isotherm plot of which are given in Table 3, respectively, give information about the suitability of adsorbent/adsorbate system and adsorption system [67–69]. If $n < 1$, the adsorption system is more heterogeneous, and the adsorption is more efficient at high concentrations. If n is equal to unity, the adsorption is linear. When $n > 1$, this indicates that the system is more efficient at low concentrations [67,68,70,71].

3.6. Adsorption kinetics

In order to explain the adsorption mechanisms in total chromium removal using $MnFe_2O_4$ NPs, the

Table 3
Langmuir, Freundlich, Temkin, and Dubinin–Radushkevich isotherm parameters

Langmuir			Freundlich			
q_m (mg/g)	K (L/mg)	R^2	K_F (mg/g)	n		R^2
500.00	0.0005	0.756	0.317	1.059		0.997
Temkin			**Dubinin–Radushkevich**			
K_T (L/mg)	b	R^2	q_d (mg/g)	β	E (kJ/mol)	R^2
0.038	118.94	0.955	34.39	0.00031	40.16	0.876

Table 4
Comparison of $q_{e,cal}$ and chi-square (χ^2) for Freundlich and Temkin isotherms

		$q_{e,cal}$		Chi-square (χ^2)	
C_e (mg/l)	q_e (mg/g)	Freundlich	Temkin	Freundlich	Temkin
36.2	9.2	9.385991	6.953931	0.003686	0.725464
71.8	18.8	17.91599	20.97915	0.043619	0.226354
110	26.66	26.79995	29.71584	0.000731	0.314248
184.95	43.36	43.76819	40.35735	0.003807	0.223402
			Total χ^2	0.051842	1.489468

Table 5
Kinetic parameters for the adsorption of Total Cr

Pseudo-first-order				Pseudo-second-order			
R^2	k_1	$q_{e,cal}$	$q_{e,exp}$	R^2	k_2	$q_{e,cal}$	$q_{e,exp}$
0.956	0.0058	21.35	89.18	0.998	0.0016	85.47	89.18

pseudo-first-order and pseudo-second-order kinetic models were used. The kinetic parameters and the correlation coefficients for the absorption of total chromium are presented in Table 5. As it is seen from Table 5, the correlation coefficient calculated from the pseudo-second-order model was high (0.998) for total chromium removal, and the calculated $q_{e,cal}$ values from the pseudo-second-order model were in good agreement with the experimental q_e values.

According to the results of Table 5, the total chromium adsorption of $MnFe_2O_4$ NPs followed a pseudo-second-order kinetic model. A plot of pseudo-second-order adsorption kinetic model for total chromium removal is shown in Fig. 6.

Intraparticle diffusion plot q_t vs. $t^{0.5}$ is represented in Fig. 7. According to this plot, the adsorption of total chromium by $MnFe_2O_4$ NPs is occurred in two phases. The initial linear section represents a gradual adsorption stage where intraparticle or pore diffusion is rate limiting and the second section of the plot represents the final equilibrium stage. Since the graph does not pass through the origin, the intraparticle diffusion is not the only rate-limiting step on the adsorption process. Therefore, the multiple diffusion model was determined to be effective in adsorption. Also, the intraparticle diffusion rate k_i and plot intercept value C were found 1.20 ((mg/g) $min^{0.5}$) and 65.03 (for total Cr), respectively. According to the results of kinetic study, it can also be suggested that the adsorption mechanism is controlled by chemical adsorption.

As shown in Table 6, the absorption capacity values obtained in this work are larger or comparable to other adsorbents reported in the literature (Table 6).

Table 6
Adsorption capacities of different adsorbents for chromium

Adsorbents	Cr(VI)	Cr(III)	Total Cr	Refs.
Plum tree bark	100–105 mg/g	–	74.4 mg/g	[12]
α-Fe_2O_3 nanofibers	16.7 mg/g	–	–	[21]
Magnetic natural zeolite–polypyrrole (MZ-PPy) composite	434.78 mg/g	–	–	[72]
Schinus molle bark	97.56 mg /g	–	73.18 mg / g	[73]
Magnetite nanospheres with hollow interiors	9 mg/g	–	–	[74]
Agroforestry wastes (fern (FE), rice husk (RI), and oak leaves)	19.25 mg/g	–	–	[75]
Core–shell polyaniline/polystyrene nanocomposite	19 mg/g	–	–	[76]
Coconut shell activated carbon	1.99 mg/g	–	–	[77]
Activated carbon was prepared from longan seed	35.02 mg/g	–	–	[78]
A highly mesoporous melamine–formaldehyde resin (MMF)	66.65 mg/g	–	–	[79]
Sunflower stem carbon−calcium alginate beads (SSC-CAB) (a down flow fixed bed column)	53.4 mg/g	–	–	[80]
Nanoparticles of $MnFe_2O_4$	–	–	89.18 mg/g	This work

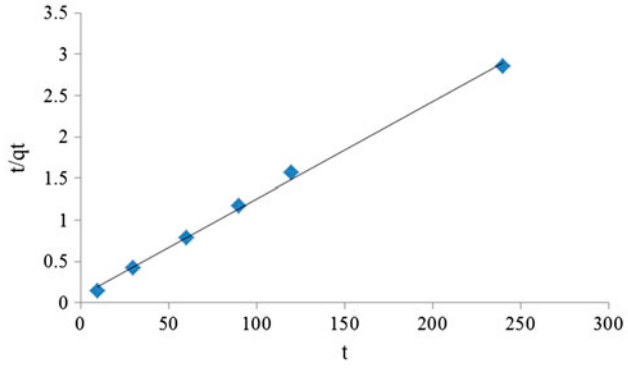

Fig. 6. A plot of t/q vs. time according to pseudo-second-order adsorption kinetics.

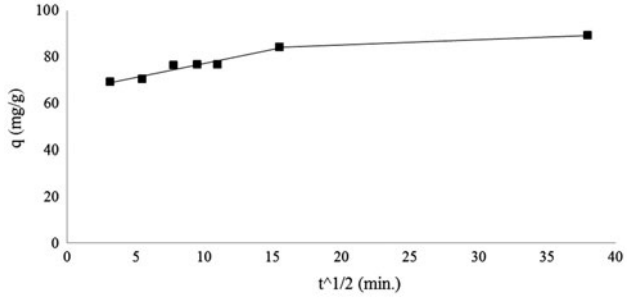

Fig. 7. Intraparticle diffusion plot for total Cr adsorption on $MnFe_2O_4$ NPs.

4. Conclusions

In this study, the total chromium removal was investigated using a novel adsorbent of $MnFe_2O_4$ NPs synthesized by a simple microwave-induced combustion technique. The $MnFe_2O_4$ NPs was provided through an efficient, quick, and inexpensive method for the removal of total chromium from galvanotechnique industry wastewater. The adsorption process was fast and the equilibrium could be reached within 120 min. And the pseudo-second-order model was the most suitable kinetic model, and intra-particle diffusion was not the only rate-limiting step on the adsorption process. The isotherm analysis indicated that the sorption data could be well represented by Freundlich isotherm model. As a result, this study showed that $MnFe_2O_4$ NPs would be a potential candidate as a high efficient and inexpensive adsorbent for the total chromium removal from real industrial wastewater.

Acknowledgement

This work was supported by Scientific Research Projects Coordination Unit of Istanbul University. Project number 28461.

List of symbols

- $1/n$ — the adsorption intensity that ranges between 0 and 1, where zero represents maximum heterogeneity of adsorbent surface
- β — the Dubinin–Radushkevich isotherm constant related to sorption the mean free energy (mol^2/kJ^2)
- ε — the Polanyi potential
- χ^2 — chi-square
- B_T — the Temkin constant related to adsorption energy (kJ/mol)
- C — the intercept
- C_e — (1) metal concentrations in the solution after the experiment (mg/L) (2) the equilibrium concentration of the adsorbate (mg/L)
- C_0 — the initial concentration of metal in the wastewater (mg/L)
- E per molecule of adsorbate
- k_1 the rate constant of pseudo-first-order adsorption (min^{-1})
- k_2 the equilibrium rate constant of pseudo-second-order adsorption (g/mg min)
- k_i the intra-particle diffusion rate constant ($(mg/g)\ min^{0.5}$)
- K_L the Langmuir isotherm constant related to the adsorption energy (L/mg)
- K_F — the Freundlich isotherm constant related to the adsorption capacity of the adsorbent (mg/g)
- K_T — the binding constant at equilibrium corresponding to the maximum binding energy (L/mg)
- m — the amount of $MnFe_2O_4$ NPs used (g)
- q_d — the theoretical isotherm saturation capacity (mg/g)
- q_e — the amount of adsorbate adsorbed per unit mass of adsorbent at equilibrium (mg/g)
- $q_{e,cal}$ — the equilibrium capacity (mg/g) calculated from model and q_e is the equilibrium capacity (mg/g) obtained from the experimental data
- q_m — the theoretical maximum monolayer adsorption capacity of the adsorbent (mg/g)
- q_t — are the adsorption amounts of heavy metal ions per gram of adsorbent at time t (min)
- R — the gas constant (8,314 J/mol K)
- R^2 — correlation coefficient
- t — the time (min)
- T — the absolute temperature (K)
- V — the sample volume (L)

References

[1] A.M. Patel, R.G. Patel, M.P. Patel, Nickel and copper removal study from aqueous solution using new cationic poly[acrylamide/N,N-DAMB/N,N-DAPB] super absorbent hydrogel, J. Appl. Polym. Sci. 119 (2011) 2485–2493.

[2] S. Mahdavi, M. Jalali, A. Afkhami, Heavy metals removal from aqueous solutions using TiO_2, MgO, and Al_2O_3 nanoparticles, Chem. Eng. Commun. 200 (2013) 448–470.
[3] M.S. Rahman, M.R. Islam, Effects of pH on isotherms modeling for Cu(II) ions adsorption using maple wood sawdust, Chem. Eng. J. 149 (2009) 273–280.
[4] A.N. Knobel, A.E. Lewis, A mathematical model of a high sulphate wastewater anaerobic treatment system, Water Res. 36 (2002) 257–265.
[5] B.H. Southichak, K. Nakano, M. Nomura, N. Chiba, O. Nishimura, Phragmites australis: A novel biosorbent for the removal of heavy metals from aqueous solution, Water Res. 40 (2006) 2295–2302.
[6] I.J. Puentes-Cárdenas, A.M. Pedroza-Rodríguez, M. Navarrete-López, T.L. Villegas-Garrido, E. Cristiani-Urbina, Biosorption of trivalent chromium from aqueous solutions by Pleurotusostreatus biomass, Environ. Eng. Manage. J. 11 (2012) 1741–1752.
[7] J. Barnhart, Occurrences, uses, and properties of chromium, Regul. Toxicol. Pharm. 26 (1997) S3–S7
[8] D. Mohan, C.U. Pittman Jr., Activated carbons and low cost adsorbents for remediation of tri- and hexavalent chromium from water, J. Hazard. Mater. 137 (2006) 762–811.
[9] D. Park, Y.S. Yun, D.S. Lee, J.M. Park, Optimum condition for the removal of Cr(VI) or total Cr using dried leaves of *Pinus densiflora*, Desalination 271 (2011) 309–314.
[10] M. Ahmaruzzaman, Role of fly ash in the removal of organic pollutants from wastewater, Energy Fuels 23 (2009) 1494–1511.
[11] T.A. Kurniawan, G.Y.S. Chan, W. Lo, S. Babel, Comparisons of low-cost adsorbents for treating wastewaters laden with heavy metals, Sci. Total Environ. 366 (2–3) (2006) 409–426.
[12] P.V. Lopez-Nuñez, E. Aranda-García, M. del C. Cristiani-Urbina, L. Morales-Barrera, E. Cristiani-Urbina, Removal of hexavalent and total chromium from aqueous solutions by plum (p. Domestica l.) tree bark, Environ. Eng. Manage. J. 13(8) (2014) 1927–1938.
[13] N. Atar, A. Olgun, S. Wang, Adsorption of cadmium (II) and zinc(II) on boron enrichment process waste in aqueous solutions: Batch and fixed-bed system studies, Chem. Eng. J. 192 (2012) 1–7.
[14] E. Osma, M. Serin, Z. Leblebici, A. Aksoy, Heavy metals accumulation in some vegetables and soils in Istanbul, Ekoloji 21 (2012) 1–8.
[15] A. Predescu, A. Nicolae, Adsorption of Zn, Cu and Cd from wastewaters by means of maghemite nanoparticles, U.P.B. Sci. Bull., Ser. B 74 (2012) 255–264.
[16] S. Chen, J. Hong, H. Yang, J. Yang, Adsorption of uranium(VI) from aqueous solution using a novel graphene oxide-activated carbon felt composite, J. Environ Radioact. 126 (2013) 253–258.
[17] H. Omar, H. Arida, A. Daifullah, Adsorption of $_{60}$Co radionuclides from aqueous solution by raw and modified bentonite, Appl. Clay Sci. 44 (2009) 21–26.
[18] C.K. Ahn, D. Park, S.H. Woo, J.M. Park, Removal of cationic heavy metal from aqueous solution by activated carbon impregnated with anionic surfactants, J. Hazard. Mater. 164 (2009) 1130–1136.
[19] N. Rajic, D. Stojakovic, M. Jovanovic, N.Z. Logar, M. Mazaj, V. Kaucic, Removal of nickel(II) ions from aqueous solutions using the natural clinoptilolite and preparation of nano-NiO on the exhausted clinoptilolite, Appl. Surf. Sci. 257 (2010) 1524–1532.
[20] M.A. Barakat, New trends in removing heavy metals from industrial wastewater, Arab. J. Chem. 4 (2010) 361–377.
[21] T. Ren, P. He, W. Niu, Y. Wu, L. Ai, X. Gou, Synthesis of α-Fe_2O_3 nanofibers for applications in removal and recovery of Cr(VI) from wastewater, Environ. Sci. Pollut. Res. 20 (2013) 155–162.
[22] N. Sezgin, M. Sahin, A. Yalcin, Y. Koseoglu, Synthesis, characterization and the heavy metal removal efficiency of MFe_2O_4 (M = Ni, Cu) nanoparticles, Ekoloji 89 (2013) 89–96.
[23] Y.C. Sharma, V. Srivastava, V.K. Singh, S.N. Kaul, C.H. Weng, Nano-adsorbents for the removal of metallic pollutants from water and wastewater, Environ. Technol. 30 (2009) 583–609.
[24] U. Wingenfelder, C. Hansen, G. Furrer, R. Schulin, Removal of heavy metals from mine waters by natural zeolites, Environ. Sci. Technol. 39 (2005) 4606–4613.
[25] A. Afkhami, M. Saber-Tehrani, H. Bagheri, Simultaneous removal of heavy metal ions in wastewater samples using nano-alumina modified with 2,4-dinitrophenylhydrazine, J. Hazard. Mater. 181 (2010) 836–844.
[26] A. Afkhami, H. Bagheri, T. Madrakian, Alumina nanoparticles grafted with functional groups as a new adsorbent in efficient removal of formaldehyde from water samples, Desalination 281 (2011) 151–158.
[27] S. Mahdavi, M. Jalali, A. Afkhami, Removal of heavy metals from aqueous solutions using Fe_3O_4, ZnO, CuO nanoparticles, J. Nanopart. Res. 14–846 (2012) 1–18.
[28] Y.T. Meng, Y.M. Zheng, L.M. Zhang, J.Z. He, Biogenic Mn oxides for effective adsorption of Cd from aquatic environment, Environ. Pollut. 157 (2009) 2577–2583.
[29] Y. Zhang, Y. Chen, P. Westerhoff, K. Hristovski, J.C. Crittenden, Stability of commercial metal oxide nanoparticles in water, Water Res. 42 (2008) 2204–2212.
[30] M.A. Tofighy, T. Mohammadi, Adsorption of divalent heavy metal ions from water using carbon nanotube sheets, J. Hazard. Mater. 185 (2011) 140–147.
[31] A.F. Ngomsik, A. Bee, M. Draye, G. Cote, V. Cabuil, Magnetic nano- and microparticles for metal removal and environmental applications: A review, C.R. Chim. 8 (2005) 963–970.
[32] S. Recillas, A. García, E. González, E. Casals, V. Puntes, A. Sánchez, X. Font, Use of CeO_2, TiO_2 and Fe_3O_4 nanoparticles for the removal of lead from water: Toxicity of nanoparticles and derived compounds, Desalination 277 (2011) 213–220.
[33] A. Rahmani, H.Z. Mousavi, M. Fazli, Effect of nanostructure alumina on adsorption of heavy metals, Desalination 253 (2010) 94–100.
[34] D. Dimitrov, Interactions of antibody-conjugated nanoparticles with biological surfaces, Colloids Surf., A 282–283 (2006) 8–10.
[35] R. Dastjerdi, M. Montazer, A review on the application of inorganic nano-structured materials in the modification of textiles: Focus on anti-microbial properties, Colloids Surf., B 79 (2010) 5–18.

[36] Y.C. Chang, D.H. Chen, Preparation and adsorption properties of monodisperse chitosan-bound Fe_3O_4 magnetic nanoparticles for removal of Cu(II) ions, J. Colloid Interface Sci. 283 (2005) 446–451.
[37] Y. Wang, G. Morin, G. Ona-Nguema, F. Juillot, G. Calas, G.E. Brown, Distinctive arsenic(V) trapping modes by magnetite nanoparticles induced by different sorption processes, Environ. Sci. Technol. 45 (2011) 7258–7266.
[38] G. Shan, S. Yan, R.D. Tyagi, R.Y. Surampalli, T. Zhang, Applications of nanomaterials in environmental science and engineering: Review, Pract. Period. Hazard. Toxic Radioact. Waste Manage. 13 (2009) 110–119.
[39] Y. Köseoğlu, Structural, magnetic, electrical and dielectric properties of $Mn_xNi_{1-x}Fe_2O_4$ spinel nanoferrites prepared by PEG assisted hydrothermal method, Ceram. Int. 39(4) (2013) 4221–4230.
[40] Y. Köseoğlu, Rapid synthesis of nanocrystalline $NiFe_2O_4$ and $CoFe_2O_4$ powders by a microwave-assisted combustion method, J. Supercond. Novel Magn. 26 (2013) 1391–1396.
[41] M. Sertkol, Y. Köseoğlu, A. Baykal, H. Kavas, A. Bozkurt, M.S. Toprak, Microwave synthesis and characterization of Zn-doped nickel ferrite nanoparticles, J. Alloys Compd. 486 (2009) 325–329.
[42] M. Sertkol, Y. Köseoğlu, A. Baykal, H. Kavas, M.S. Toprak, Synthesis and magnetic characterization of $Zn_{0.7}Ni_{0.3}Fe_2O_4$ nanoparticles via microwave assisted combustion route, J. Magn. Magn. Mater. 322 (2010) 866–871.
[43] H. Imam Maarof, B.H. Hameed, A.L. Ahmad, Adsorption equilibrium of phenols from aqueous Solution using modified clay, J. Jurutera Kimia Malaysia 3 (1996) 85–176.
[44] I. Langmuir, The adsorption of gases on plane surfaces of glass, mica and platinum, J. Am. Chem. Soc. 40 (1908) 1361–1403.
[45] H.M.F. Freundlich, Über die adsorption in lösungen, Z. Phys. Chem 57 (1906) 385–470.
[46] A. Günay, E. Arslankaya, İ. Tosun, Lead removal from aqueous solution by natural and pretreated clinoptilolite: Adsorption equilibrium and kinetics, J. Hazard. Mater. 146 (2007) 362–371.
[47] A. Dąbrowski, Adsorption—From theory to practice, Adv. Colloid Interface Sci. 93 (2001) 135–224.
[48] M. Özacar, Equilibrium and kinetic modeling of adsorption of phosphorus on calcined alunite, Adsorption 9 (2003) 2125.
[49] M.I. Tempkin, V. Pyzhev, Kinetics of ammonia synthesis on promoted iron catalyst, Acta Phys.-Chim. 12 (1940) 327–356.
[50] S. Lagergren, Zurtheorie der sogenannten adsorption gelösterstoffe, K. Vet. Akad. Handl. 24(4) (1898) 1–39.
[51] K.K. Singh, R. Rastogi, S.H. Hasan, Removal of Cr(VI) from wastewater using rice bran, J. Colloid Interface Sci. 290 (2005) 61–68.
[52] H.K. Boparai, M. Joseph, D.M. O'Carroll, Kinetics and thermodynamics of cadmium ion removal by adsorption onto nano zerovalent iron particles, J. Hazard. Mater. 186 (2011) 458–465.
[53] P. Chingombe, B. Saha, R.J. Wakeman, Sorption of atrazine on conventional and surface modified activated carbons, J. Colloid Interface Sci. 302 (2006) 408–416.
[54] S.I.H. Taqvi, S.M. Hasany, M.I. Bhanger, Sorption profile of Cd(II) ions onto beach sand from aqueous solutions, J. Hazard. Mater. 141 (2007) 37–44.
[55] D. Kavitha, C. Namasivayam, Experimental and kinetic studies on methylene blue adsorption by coir pith carbon, Bioresour. Technol. 98 (2007) 14–21.
[56] A. Ozcan, A.S. Ozcan, O. Gok, Adsorption kinetics and isotherms of anionic dye of reactive blue 19 from aqueous solutions onto DTMA-sepiolite, in: A.A. Lewinsky (Ed.), Hazardous Materials and Wastewater —Treatment, Removal and Analysis, Nova Science Publishers, New York, NY, 2007, pp. 225–249.
[57] E.I. Unuabonah, K.O. Adebowale, B.I. Olu-Owolabi, Kinetic and thermodynamic studies of the adsorption of lead(II) ions onto phosphate-modified kaolinite clay, J. Hazard. Mater. 144 (2007) 386–395.
[58] F.C. Wu, R.L. Tseng, R.S. Juang, Initial behavior of intraparticle diffusion model used in the description of adsorption kinetics, Chem. Eng. J. 153 (2009) 1–8.
[59] M. Günay, H. Erdemi, A. Baykal, H. Sözeri, M.S. Toprak, Triethylene glycol stabilized $MnFe_2O_4$ nanoparticle: Synthesis, magnetic and electrical characterization, Mater. Res. Bull. 48 (2013) 1057–1064.
[60] Y. Köseoğlu, F. Alan, M. Tan, R. Yilgin, M. Öztürk, Low temperature hydrothermal synthesis and characterization of Mn doped cobalt ferrite nanoparticles, Ceram. Int. 38 (2012) 3625–3634.
[61] V.K. Garg, R. Kumar, R. Gupta, Removal of malachite green dye from aqueous solution by adsorption using agro-industry waste: A case study of Prosopis cineraria, Dyes Pigm. 62 (2004) 1–12.
[62] H. Chen, A. Wang, Adsorption characteristics of Cu(II) from aqueous solution onto poly(acrylamide)/attapulgite composite, J. Hazard. Mater. 165 (2009) 223–231.
[63] M. Xu, Y. Zhang, Z. Zhang, Y. Shen, M. Zhao, G. Pan, Study on the adsorption of Ca^{2+}, Cd^{2+}, and Pb^{2+} by magnetic Fe_3O_4 yeast treated with EDTA dianhydride, Chem. Eng. J. 168 (2011) 737–745.
[64] A. Özer, D. Özer, A. Özer, The adsorption of copper (II) ions on to dehydrated wheat bran (DWB): Determination of the equilibrium and thermodynamic parameters, Process Biochem. 39 (2004) 2183–2191.
[65] A.K. Agarwal, M.S. Kadu, C.P. Pandhurnekar, I.L. Muthreja, Langmuir, Freundlich and BET adsorption isotherm studies for zinc ions onto coal fly ash, Int. J. Appl. Innov. Eng. Manage. (IJAIEM) 3(1) (2014) 64–71.
[66] J.C.Y. Ng, W.H. Cheung, G. McKay, Equilibrium studies for the sorption of lead from effluents using chitosan, Chemosphere 52 (2003) 1021–1030.
[67] T.S. Anirudhan, P.S. Suchithra, Equilibrium, kinetic and thermodynamic modeling for the adsorption of heavy metals onto chemically modified hydrotalcite, Indian J. Chem. Technol. 17 (2010) 247–259.
[68] R. Donat, A. Akdogan, E. Erdem, H. Cetisli, Thermodynamics of Pb^{2+} and Ni^{2+} adsorption onto natural bentonite from aqueous solutions, J. Colloid Interface Sci. 286 (2005) 43–52.
[69] L. Monser, N. Adhoum, Modified activated carbon for the removal of copper, zinc, chromium, and cyanide from wastewater, Sep. Purif. Technol. 26 (2002) 137–146.
[70] S. Babel, T.A. Kurniawan, Cr(VI) removal from synthetic wastewater using coconut shell charcoal and commercial activated carbon modified with oxidizing agents and/or chitosan, Chemosphere 54 (2004) 951–967.

[71] N. Balkaya, H. Cesur, Adsorption of cadmium from aqueous solution by phosphogypsum, Chem. Eng. J. 140 (2008) 247–254.
[72] N.H. Mthombeni, S. Mbakop, M.S. Onyango, Magnetic zeolite-polymer composite as an adsorbent for the remediation of wastewaters containing vanadium, Int. J. Environ. Sci. Dev. 6(8) (2015) 602–605.
[73] A.R. Netzahuatl-Muñoz, E. Aranda-García, M. del C. Cristiani-Urbina, B.E. Barragán-Huerta, T.L. Villegas-Garrido, E. Cristiani-Urbina, Removal of hexavalent and total chromium from aqueous solutions by Schinus molle bark, Fresen. Environ. Bull. 19(12) (2010) 2911–2918.
[74] M. Kumari, C.U. Pittman, D. Mohan, Heavy metals [chromium(VI) and lead(II)] removal from water using mesoporous magnetite (Fe_3O_4) nanospheres, J. Colloid Interface Sci. 442 (2015) 120–132.
[75] E. Rosales, L. Ferreira, M.Á. Sanromán, T. Tavares, M. Pazos, Enhanced selective metal adsorption on optimised agroforestry waste mixtures, Bioresour. Technol. 182 (2015) 41–49.
[76] M.S. Lashkenari, B. Davodi, M. Ghorbani, H. Eisazadeh, Use of core–shell polyaniline/polystyrene nanocomposite for removal of Cr(VI), High Perform. Polym. 24 (2012) 1–11.
[77] Y. Wu, P. Yilihan, J. Cao, Y. Jin, Competetive adsorption of Cr(VI) and Ni(II) onto coconut shell activated carbon in single and binary systems, Water Air Soil Pollut. 224(1662) (2013) 1–13.
[78] J. Yang, M. Yu, W. Chen, Adsorption of hexavalent chromium from aqueous solution by activated carbon prepared from longan seed: Kinetics, equilibrium and thermodynamics, J. Ind. Eng. Chem. 21 (2015) 414–422.
[79] Z. Lv, C. Liang, J. Cui, Y. Zhang, S. Xu, A facile route for the synthesis of mesoporous melamine-formaldehyde resins for hexavalent chromium removal, RSC Adv. 5 (2015) 18213–18217.
[80] M. Jain, V.K. Garg, K. Kadirvelu, M. Sillanpää, Combined effect of sunflower stem carbon-calcium alginate beads for the removal and recovery of chromium from contaminated water in column mode, Ind. Eng. Chem. Res. 54(5) (2015) 1419–1425.